

Stern-Gerlach deflection of optical Thirring solitons in a coherent atomic system

Zhiming Chen,^{1,2,*} Hongqiang Xie,² Qun Li,² and Guoxiang Huang^{3,4}

¹State Key Laboratory of Nuclear Resources and Environment, East China University of Technology, Nanchang 330013, Jiangxi, China

²School of Science, East China University of Technology, Nanchang 330013, Jiangxi, China

³State Key Laboratory of Precision Spectroscopy, School of Physical and Material Sciences, East China Normal University, Shanghai 200062, China

⁴NYU-ECNU Joint Institute of Physics, New York University at Shanghai, Shanghai 200062, China



(Received 24 March 2019; revised manuscript received 14 June 2019; published 15 July 2019)

We propose a scheme to realize an optical Thirring model and create temporal optical Thirring solitons in a tripod-type atomic gas via double electromagnetically induced transparency (EIT). We show that giant enhancement of the cross-phase modulation for the two polarization components of the probe pulse can be obtained under the condition of the double EIT, and hence the optical Thirring model can be realized. We also show that the system supports stable temporal optical Thirring solitons, which have ultralow generation power and ultraslow propagation velocity. In particular, these temporal optical Thirring solitons may experience a significant Stern-Gerlach deflection when a gradient magnetic field is applied to the system. The results reported here are useful not only for extending the research realm of nonlinear magneto-optics but also for the application in precision measurements, such as the detection of microgradient magnetic fields.

DOI: [10.1103/PhysRevA.100.013827](https://doi.org/10.1103/PhysRevA.100.013827)

I. INTRODUCTION

The Thirring model was first proposed by W. Thirring in 1953 [1]. The specific character of this model is that the interaction between particles is described by cross-phase modulation (CPM). The Thirring model is a standard nonlinear model in quantum field theory. In addition to earlier studies (see the review [2] and references therein), there have been many research activities on its quantum integrability and related quantum solitons [3–6]. Subsequent studies have shown that the Thirring model can be used to describe exceptional electronic properties of graphene and superconducting materials [7–13] and nonlinear behaviors of matter waves in Bose-Einstein condensates [14–16].

In recent years, much attention has been paid to the research on optical Thirring solitons that occur in many nonlinear optical materials, such as photorefractive crystals [17,18], quadratic optical media [19–21], birefringent fibers [22–25], laser-driven atomic gases [26–28], and quantum wells [29] via electromagnetically induced transparency (EIT). Although these interesting research advances are very useful for the understanding of optical Thirring solitons in various nonlinear optical systems, it is desirable to find optical Thirring solitons that can be actively manipulated and are promising for practical applications.

In this work, we suggest a physical scheme to realize a *temporal optical Thirring model* and generate *temporal optical Thirring solitons*. The system we consider is a tripod-type four-level atomic gas working under condition of double EIT. We demonstrate that under the condition of the double EIT the optical Kerr nonlinearity of the system can be enhanced greatly and the CPM in the two polarization components of

the probe laser pulse can be made to be much larger than the self-phase modulation (SPM), and hence the optical Thirring model can be realized. Moreover, we prove that the system supports stable temporal optical Thirring solitons, which have ultralow generation power ($\sim 10^{-9}$ W) and ultraslow, well-matched propagation velocities ($\sim 10^{-4}c$, where c is the light speed in vacuum) for the two polarization components; in particular, these temporal optical Thirring solitons may experience a Stern-Gerlach (SG) deflection and acquire a significant deflection angle when a gradient magnetic field is applied to the system.

Before proceeding, we point out that the optical Thirring solitons obtained here are different from those reported before. First, the optical Thirring solitons proposed in Refs. [17–25] were based on various passive optical media, and most of them are spatial optical solitons (i.e., stationary nonlinear optical beams in space). Such optical Thirring solitons generally have large generation power and are not easy to manipulate actively. Second, although the optical Thirring solitons studied in Refs. [26–29] are ones with low generation power based on EIT schemes, all of them are spatial optical Thirring solitons and also have lower controllability. In contrast, the optical Thirring solitons presented in our work are temporal ones (i.e., nonlinear optical pulses propagating in space and time), and their time-dependent movement trajectories can be actively manipulated and controlled by virtue of SG gradient magnetic fields. The research results obtained here are not only useful for developing nonlinear magneto-optics but also promising for practical applications in precision measurements (e.g., the detection of micro gradient magnetic fields) and in optical information processing and transmission.

The rest of the article is arranged as follows. In Sec. II, we present the theoretical model under study. In Sec. III, we derive coupled nonlinear envelope equations of the two

*czmhnu@163.com

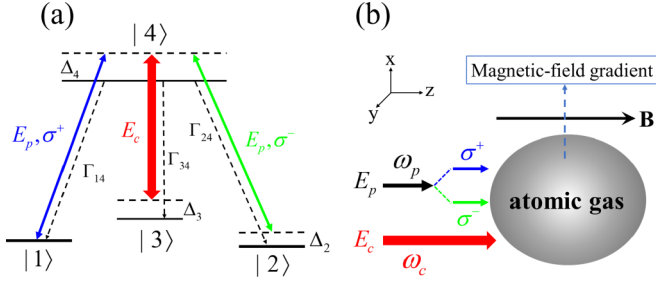


FIG. 1. (a) Double-EIT excitation scheme of the four-level atomic system. A weak, pulsed probe laser field E_p couples the levels $|1\rangle$ and $|4\rangle$ ($|2\rangle$ and $|4\rangle$) by its σ^+ (σ^-) polarization component; a strong, continuous-wave control laser field E_c couples the levels $|3\rangle$ and $|4\rangle$. Atoms are assumed to be initially prepared in ground states $|1\rangle$ and $|2\rangle$. Δ_2 , Δ_3 , and Δ_4 are detunings. Γ_{14} , Γ_{24} , and Γ_{34} are the spontaneous emission decay rates from $|4\rangle$ to $|1\rangle$, $|4\rangle$ to $|2\rangle$, and $|4\rangle$ to $|3\rangle$, respectively. (b) Possible experimental arrangement of beam geometry. The probe and control fields (with angular frequency ω_p and ω_c , respectively) propagate along the z direction. A Stern-Gerlach magnetic field \mathbf{B} is applied along the z direction with its gradient along the x direction.

polarization components of the probe pulse, describe the realization of the optical Thirring model, and give solutions of temporal optical Thirring solitons. In Sec. IV, we study the Stern-Gerlach deflection of the optical Thirring solitons. Finally, in Sec. V a summary on the main results obtained in this work is given.

II. MODEL

We consider a lifetime-broadened atomic gas with a tripod-type four-level configuration, interacting resonantly with two laser fields [see Fig. 1(a)]. A linearly polarized, pulsed probe laser field \mathbf{E}_p with the center frequency $\omega_p/(2\pi)$ couples the transitions $|1\rangle \leftrightarrow |4\rangle$ ($|2\rangle \leftrightarrow |4\rangle$) by its σ^+ polarization component (σ^- polarization component); a π -polarized, strong continuous-wave control laser field \mathbf{E}_c with the center frequency $\omega_c/(2\pi)$ couples the transition $|3\rangle \leftrightarrow |4\rangle$. Atoms are assumed to be cooled to an ultralow temperature so that their center-of-mass motion is negligible, and they are prepared initially in the ground states $|1\rangle$ and $|2\rangle$. This tripod-type system can be taken to be two Λ -type systems, i.e., $|1\rangle \leftrightarrow |3\rangle \leftrightarrow |4\rangle$ and $|2\rangle \leftrightarrow |3\rangle \leftrightarrow |4\rangle$, sharing the levels $|3\rangle$ and $|4\rangle$, which results in double EIT [30].

A possible arrangement for measuring the temporal optical Thirring solitons and their SG deflection is shown in Fig. 1(b). For simplicity, the probe and control fields are assumed to propagate along the z direction, and thus the electric-field vector can be written as $\mathbf{E} = \mathbf{E}_p + \mathbf{E}_c = \hat{\mathbf{e}}_+ \mathcal{E}_p e^{i(k_p z - \omega_p t)} + \hat{\mathbf{e}}_- \mathcal{E}_p e^{i(k_p z - \omega_p t)} + \hat{\mathbf{e}}_c \mathcal{E}_c e^{i(k_c z - \omega_c t)} + \text{c.c.}$ Here $\hat{\mathbf{e}}_+ = (\hat{\mathbf{e}}_x + i\hat{\mathbf{e}}_y)/\sqrt{2}$ [$\hat{\mathbf{e}}_- = (\hat{\mathbf{e}}_x - i\hat{\mathbf{e}}_y)/\sqrt{2}$] is the unit vector of the σ^+ - (σ^-) polarization component of the probe field with the envelope \mathcal{E}_p (\mathcal{E}_p), $\hat{\mathbf{e}}_x$ ($\hat{\mathbf{e}}_y$) is the unit vector along the coordinate axis x (y), $\hat{\mathbf{e}}_c$ is the unit vector of the control field with the envelope \mathcal{E}_c , and $k_p = \omega_p/c$ ($k_c = \omega_c/c$) is the wave number of the probe (control) field before entering the atomic gas. Additionally, an

SG gradient magnetic field with the form

$$\mathbf{B}(x) = \hat{\mathbf{e}}_z Bx \quad (1)$$

is applied to the system which is used to realize a trajectory manipulation of the probe pulse, as will be shown in Sec. IV. Here $\hat{\mathbf{e}}_z$ is the unit vector in the z direction and B characterizes the transverse gradient of the applied magnetic field. Due to the presence of the SG gradient magnetic field, the Zeeman level shift $\Delta E_{j, \text{Zeeman}} = \mu_B g_F^j m_F^j Bx$ for the level $|j\rangle$ occurs. Here μ_B , g_F^j , and m_F^j are Bohr magneton, gyromagnetic factor, and magnetic quantum number of the atomic state $|j\rangle$, respectively.

Under the electric-dipole and rotating-wave approximations, the Hamiltonian of the system in the interaction picture reads

$$\hat{\mathcal{H}} = - \sum_{j=1}^4 \hbar \Delta'_j |j\rangle \langle j| - \hbar [\Omega_c |4\rangle \langle 3| + \Omega_{p1} |4\rangle \langle 1| + \Omega_{p2} |4\rangle \langle 2| + \text{H.c.}], \quad (2)$$

with $\Delta'_j = \Delta_j - \mu_{j1} Bx$, $\mu_{j1} = \mu_B (g_F^j m_F^j - g_F^1 m_F^1)/\hbar$, $\Omega_c = (\mathbf{p}_{34} \cdot \hat{\mathbf{e}}_c) \mathcal{E}_c / \hbar$, $\Omega_{p1} = (\mathbf{p}_{14} \cdot \hat{\mathbf{e}}_+) \mathcal{E}_p / \hbar$, and $\Omega_{p2} = (\mathbf{p}_{24} \cdot \hat{\mathbf{e}}_-) \mathcal{E}_p / \hbar$, with \mathbf{p}_{jl} being the electric dipole matrix element associated with the transition from $|j\rangle$ to $|l\rangle$. Here Ω_{p1} and Ω_{p2} are half Rabi frequencies of the two circularly polarized components of the probe field, while Ω_c is the half Rabi frequency of the π -polarized control field; $\Delta_1 = 0$, $\Delta_2 = -\omega_{21}$, $\Delta_3 = \omega_p - \omega_c - \omega_{31}$, and $\Delta_4 = \omega_p - \omega_{41}$ are the detunings, where $\omega_{jl} = (E_j - E_l)/\hbar$ with E_j being the eigenenergy of the state $|j\rangle$.

The equation of motion for density matrix σ in the interaction picture is [31]

$$\frac{\partial \sigma}{\partial t} = -\frac{i}{\hbar} [\hat{\mathcal{H}}, \sigma] - \Gamma[\sigma], \quad (3)$$

where σ is a 4×4 density matrix in the interaction picture and Γ is a 4×4 relaxation matrix denoting the spontaneous emission and dephasing of the system. The explicit expression for density matrix elements σ_{jl} is presented in Appendix A.

The equation of motion for the probe-field Rabi frequencies Ω_{pj} can be captured by the Maxwell equation $\nabla^2 \mathbf{E} - (1/c^2) \partial^2 \mathbf{E} / \partial t^2 = [1/(\epsilon_0 c^2)] \partial^2 \mathbf{P} / \partial t^2$. The electric polarization intensity of the system is given by $\mathbf{P}(\mathbf{r}, t) = \mathcal{N}_a \{\mathbf{p}_{14} \sigma_{41} \exp[i(k_p z - \omega_p t)] + \mathbf{p}_{24} \sigma_{42} \exp[i(k_p z - \omega_p t)] + \mathbf{p}_{34} \sigma_{43} \exp[i(k_c z - \omega_c t)] + \text{c.c.}\}$, with \mathcal{N}_a being atomic density. Under slowly varying envelope approximation the Maxwell equation is reduced to

$$i \left(\frac{\partial}{\partial z} + \frac{1}{c} \frac{\partial}{\partial t} \right) \Omega_{pj} + \frac{c}{2\omega_p} \frac{\partial^2}{\partial x^2} \Omega_{pj} + \kappa_{j4} \sigma_{4j} = 0, \quad (j = 1, 2), \quad (4)$$

where $\kappa_{14} = \mathcal{N}_a \omega_p |\mathbf{p}_{14} \cdot \hat{\mathbf{e}}_+|^2 / (2\hbar \epsilon_0 c)$ and $\kappa_{24} = \mathcal{N}_a \omega_p |\mathbf{p}_{24} \cdot \hat{\mathbf{e}}_-|^2 / (2\hbar \epsilon_0 c)$. Note that we have assumed that the transverse radius of the probe field in the y direction is large enough so that the diffraction in the y direction is negligible.

The model described above can be easily realized by selecting realistic physical systems. One of them is the ^{87}Rb atoms tuned to the D1-line transition with the

energy levels selected as $|1\rangle = |5^2S_{1/2}, F=1, m_F=-1\rangle$ ($g_F = -1/2$), $|2\rangle = |5^2S_{1/2}, F=2, m_F=1\rangle$ ($g_F = 1/2$), $|3\rangle = |5^2S_{1/2}, F=2, m_F=0\rangle$ ($g_F = 1/2$), and $|4\rangle = |5^2P_{1/2}, F=2, m_F=0\rangle$ ($g_F = 1/6$) [32]. The decay rates are given by $\Gamma_2 \simeq \Gamma_3 \simeq 2\pi \times 1$ kHz and $\Gamma_4 \simeq 2\pi \times 5.75$ MHz. The electric dipole matrix elements are also given by $|\mathbf{p}_{14}| \simeq |\mathbf{p}_{24}| \simeq 2.54 \times 10^{-27}$ C cm. We assume that atomic density $N_a \approx 3.69 \times 10^{10}$ cm $^{-3}$, then $\kappa_{14} \approx \kappa_{24} \approx 1.0 \times 10^9$ cm $^{-1}$ s $^{-1}$.

III. COUPLED NONLINEAR ENVELOPE EQUATIONS AND TEMPORAL OPTICAL THIRRING SOLITONS

A. Coupled nonlinear envelope equations

In order to investigate the nonlinear evolution of the probe pulse and the possible formation of the temporal optical Thirring solitons in the system, we first employ the method of multiple scales [33] to derive coupled nonlinear envelope equations of the two polarization components of the probe field based on the Maxwell-Bloch (MB) Eqs. (3) and (4). To this end, we take the asymptotic expansion $\sigma_{jl} = \sum_{\alpha=0}^{\infty} \epsilon^{\alpha} \sigma_{jl}^{(\alpha)}$ ($j, l = 1, 2, 3, 4$), $\Omega_{pm} = \sum_{\alpha=1}^{\infty} \epsilon^{\alpha} \Omega_{pm}^{(\alpha)}$ ($m = 1, 2$); we assume $B(x_1) = \epsilon^2 Bx_1$, and thus $d_{jl} = d_{jl}^{(0)} + \epsilon^2 d_{jl}^{(2)}$, with $d_{jl}^{(0)} = \Delta_j - \Delta_l + i\gamma_{jl}$ and $d_{jl}^{(2)} = -\mu_{jl} Bx_1$. Here $\sigma_{jj}^{(0)}$ is the initial population distribution prepared in the state $|j\rangle$ ($j = 1, 2$), which is assumed as $1/2$ for simplicity; ϵ is a dimensionless small parameter characterizing the typical amplitude of the probe field. All the quantities on the right-hand sides of the expansion are considered as functions of the multiscale variables $x_1 = \epsilon x$, $z_{\alpha} = \epsilon^{\alpha} z$, and $t_{\alpha} = \epsilon^{\alpha} t$ ($\alpha = 0, 2$).

Substituting the above expansion into MB Eqs. (3) and (4), and comparing the coefficients of ϵ^{α} ($\alpha = 1, 2, 3, \dots$), we obtain a set of linear but inhomogeneous equations for $\sigma_{jl}^{(\alpha)}$ and $\Omega_{pj}^{(\alpha)}$, which can be solved order by order. When carrying out the calculation of the expansion up to the third order, we obtain the following nonlinear equations for the envelopes F_j of the two polarization components of the probe pulse:

$$i\left(\frac{\partial}{\partial z_2} + \frac{1}{V_{gj}} \frac{\partial}{\partial t_2}\right)F_j + \frac{c}{2\omega_p} \frac{\partial^2}{\partial x_1^2} F_j + \sum_{l=1}^2 W_{jl} |F_l| F_j e^{-2\tilde{\alpha}_l z_2} + M_j Bx_1 F_j = 0, \quad (5)$$

($j = 1, 2$), where $\tilde{\alpha}_l = \epsilon^{-2} \alpha_l = \epsilon^{-2} \text{Im}[K_l(\omega = 0)]$, $V_{gj} = [\partial K_j(\omega)/\partial \omega]^{-1}$ is the group velocity of the j th polarization component, W_{jj} is SPM coefficient, W_{jl} ($j \neq l$) is CPM coefficient, and $M_j Bx_1$ is external potential contributed by SG gradient magnetic field. The first-order and second-order solutions of the expansion and the explicit expressions of W_{jl} and M_j are presented in Appendix B.

For the convenience of later calculations, we convert Eq. (5) into the dimensionless form

$$i\left(\frac{\partial}{\partial s} + \frac{1}{\lambda_j} \frac{\partial}{\partial \tau}\right)u_j + \frac{1}{2} \frac{\partial^2}{\partial \xi^2} u_j + \sum_{l=1}^2 g_{jl} |u_l|^2 u_j + \mathcal{M}_j \xi u_j = -ig_{Aj} u_j, \quad (6)$$

where $u_j = \epsilon F_j / U_0 e^{-\tilde{\alpha}_j z_2}$, $s = z/L_{\text{Diff}}$, $\tau = t/\tau_0$, $\lambda_j = V_{gj} \tau_0 / L_{\text{Diff}}$, $\xi = x/R$, $g_{Aj} = \alpha_j L_{\text{Diff}}$, $\mathcal{M}_j = M_j B R L_{\text{Diff}}$ ($j = 1, 2$), and $g_{jl} = W_{jl} / |W_{12}|$ ($j, l = 1, 2$). Here $L_{\text{Diff}} = \omega_p R^2 / c$, τ_0 , R , and U_0 are typical diffraction length, pulse duration, radius in the transverse direction, and Rabi frequency of the probe pulse, respectively. Following Refs. [34,35], we consider the wave-packet solution of the form

$$u_j(\tau, s, \xi) = G_j(\tau, s) v_j(\tau, \xi), \quad (7a)$$

$$G_j(\tau, s) \equiv \sqrt{2} e^{-(s-\lambda_j \tau)^2 / \rho_0^2} = \sqrt{2} e^{-(z-V_{gj}t)^2 / (\rho_0^2 L_{\text{Diff}}^2)}, \quad (7b)$$

where ρ_0 is a free real parameter. After integrating over the variable s , Eq. (6) becomes

$$\left(\frac{i}{\lambda_j} \frac{\partial}{\partial \tau} + \frac{1}{2} \frac{\partial^2}{\partial \xi^2}\right)v_j + \sum_{l=1}^2 g_{jl} |v_l|^2 v_j + \mathcal{M}_j \xi v_j = -ig_{Aj} v_j. \quad (8)$$

B. Realization of the temporal optical Thirring model

Generally, the coefficients in Eq. (8) are complex, and hence the system does not allow stable localized nonlinear solutions. Fortunately, if the system works under the condition of double EIT, then the imaginary parts of these coefficients can be made much smaller than their real parts and thus two-component optical soliton solutions are possible.

The third-order self-Kerr nonlinear optical susceptibilities $\chi_{11}^{(3)}$ and $\chi_{22}^{(3)}$ are respectively proportional to the SPM coefficients W_{11} and W_{22} in Eq. (5), while third-order cross-Kerr nonlinear optical susceptibilities $\chi_{12}^{(3)}$ and $\chi_{21}^{(3)}$ are respectively proportional to the CPM coefficients W_{12} and W_{21} . Using the parameters indicated at the end of Sec. II and choosing other realistic parameters $\Omega_c = 7.5 \times 10^7$ Hz, $\tau_0 = 6.3 \times 10^{-8}$ s, $U_0 = 5.97 \times 10^6$ Hz, $R = 30$ μm , $\Delta_2 = 0$, $\Delta_3 = -1.5 \times 10^7$ Hz, and $\Delta_4 = 8 \times 10^6$ Hz, we obtain $M_1 = M_2 \equiv M = (1.50 - 0.016i) \times 10^{-5}$ mG $^{-1}$ cm $^{-1}$, $W_{11} \approx W_{22} = (3.68 + 0.28i) \times 10^{-15}$ cm $^{-1}$ s 2 , $W_{12} \approx W_{21} = (3.97 + 0.01i) \times 10^{-14}$ cm $^{-1}$ s 2 . Based on the relations $\chi_{11}^{(3)} = \frac{2c}{\omega_p} \frac{|\mathbf{p}_{14}|^2}{\hbar^2} W_{11}$, $\chi_{22}^{(3)} = \frac{2c}{\omega_p} \frac{|\mathbf{p}_{24}|^2}{\hbar^2} W_{22}$, $\chi_{12}^{(3)} = \frac{2c}{\omega_p} \frac{|\mathbf{p}_{24}|^2}{\hbar^2} W_{12}$, and $\chi_{21}^{(3)} = \frac{2c}{\omega_p} \frac{|\mathbf{p}_{14}|^2}{\hbar^2} W_{21}$, we obtain

$$\chi_{11}^{(3)} \approx \chi_{22}^{(3)} = (5.44 + 0.42i) \times 10^{-5} \text{cm}^2 \text{V}^{-2}, \quad (9a)$$

$$\chi_{12}^{(3)} \approx \chi_{21}^{(3)} = (5.87 + 0.013i) \times 10^{-4} \text{cm}^2 \text{V}^{-2}. \quad (9b)$$

We see that there are three obvious features for the self-Kerr and cross-Kerr nonlinear optical susceptibilities. First, the real parts of these nonlinear optical susceptibilities have the order of magnitude 10^{-4} cm 2 V $^{-2}$, which is 10^{11} times larger than the third-order nonlinear optical susceptibilities found in conventional nonlinear optical media [31]. Second, the imaginary parts of these nonlinear optical susceptibilities are much smaller than their corresponding real parts, which is due to the quantum destructive interference induced by the double EIT effect. Third, the real parts of the cross-Kerr susceptibilities are 10 times larger than that of the self-Kerr susceptibilities. Thus with a short propagation distance the SPM terms in Eq. (8) may be neglected and hence only the CPM terms play significant roles, which means that an optical Thirring

model with external magnetic potential (contributed by the SG gradient magnetic field) and damping can be realized in the system, i.e., we have

$$\begin{aligned} & \left(\frac{i}{\lambda_1} \frac{\partial}{\partial \tau} + \frac{1}{2} \frac{\partial^2}{\partial \xi^2} \right) v_1 + g_{12} |v_2|^2 v_1 + \mathcal{M}_1 \xi v_1 \\ & = -i g_{A1} v_1, \end{aligned} \quad (10a)$$

$$\begin{aligned} & \left(\frac{i}{\lambda_2} \frac{\partial}{\partial \tau} + \frac{1}{2} \frac{\partial^2}{\partial \xi^2} \right) v_2 + g_{21} |v_1|^2 v_2 + \mathcal{M}_2 \xi v_2 \\ & = -i g_{A2} v_2. \end{aligned} \quad (10b)$$

Based on the system parameters given above, we obtain the typical diffraction length $L_{\text{Diff}} = 0.7$ cm, which is (for getting soliton solutions) assumed to be approximately equal to typical nonlinearity length $L_{\text{Nonl}} (\equiv 1/U_0^2 |W_{12}|)$. The typical linear absorption length $L_{A_j} = 1/\text{Im}[K_j]$ is 144.9 cm, which is (due to the double EIT effect) much larger than the typical diffraction and nonlinearity lengths L_{Diff} and L_{Nonl} . As a result, we have $\lambda_1 = \lambda_2 \approx 1 + 0.01i$, $g_{12} = g_{21} = 1 + 0.002i$, $g_{11} = g_{22} = 0.09 + 0.007i$, and $g_{A1} = g_{A2} = 0.005$; Eq. (10) in the absence of the external magnetic potential is reduced into

$$i \frac{\partial v_1}{\partial \tau} + \frac{1}{2} \frac{\partial^2 v_1}{\partial \xi^2} + |v_2|^2 v_1 = 0, \quad (11a)$$

$$i \frac{\partial v_2}{\partial \tau} + \frac{1}{2} \frac{\partial^2 v_2}{\partial \xi^2} + |v_1|^2 v_2 = 0, \quad (11b)$$

which is different from the optical Thirring model obtained before [26–29] since it involves time derivatives and hence it is a *temporal* optical Thirring model.

C. Temporal optical Thirring solitons

We now consider the formation and propagation of temporal optical Thirring soliton in the absence of the SG gradient magnetic field. Plotted in Fig. 2 is the numerical result of Eq. (10) for $\mathcal{M}_1 = \mathcal{M}_2 = 0$ by taking $|v_1|^2$ (for σ^+ -polarization component) and $|v_2|^2$ (for σ^- -polarization component) as functions of τ/τ_0 and x/R . Figure 2(a) [Fig. 2(b)] shows $|v_1|^2$ ($|v_2|^2$) when the CPM effect plays no significant role for mismatched group velocities. One sees that both $|v_1|^2$ and $|v_2|^2$ are broadened rapidly during propagation, which means in this case no soliton can be obtained. However, when the CPM effect plays a significant role and the two components have matched group velocities, $|v_1|^2$ and $|v_2|^2$ have no broadening during propagation [see Figs. 2(c) and 2(d)], i.e., in this situation a temporal optical Thirring soliton is formed in the system. In fact, Eq. (11), which is an approximate form of Eq. (10), admits the exact temporal Thirring soliton solution,

$$v_1 = v_2 = \zeta_0 \text{sech}[\zeta_0(\xi - \eta_0 \tau - \xi_0)] e^{i[\eta_0 \xi - (\eta_0^2 - \zeta_0^2)\tau/2 - \varphi_0]}, \quad (12)$$

where ζ_0 , η_0 , ξ_0 , and φ_0 are free real parameters. It is possible to get other types of temporal Thirring soliton solutions under different physical conditions.

An additional numerical simulation on the stability of the temporal optical Thirring soliton is carried out by taking the initial soliton pair as $v_1 = v_2 = \text{sech}(\xi)$, which is obtained

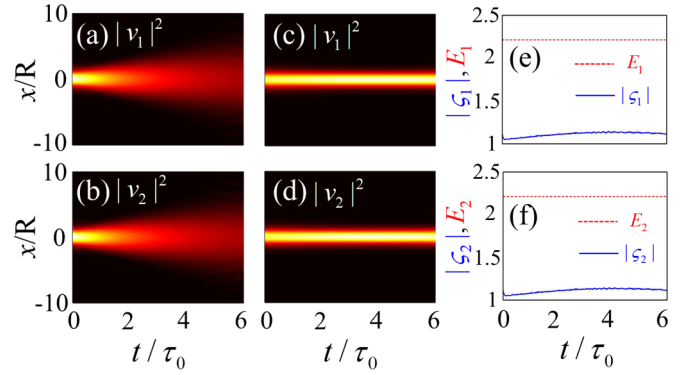


FIG. 2. Formation and propagation of temporal optical Thirring soliton by taking $|v_1|^2$ (for σ^+ -polarization component) and $|v_2|^2$ (for σ^- -polarization component) as functions of t/τ_0 and x/R . Panel (a) [(b)] is the intensity distribution $|v_1|^2$ ($|v_2|^2$) when the CPM effect plays no significant role for mismatched group velocities. Two intensity distributions ($|v_1|^2$ and $|v_2|^2$) are broadened rapidly during propagation and thus no soliton can form. Panel (c) [(d)] gives the intensity distribution $|v_1|^2$ ($|v_2|^2$) when the CPM effect plays a significant role for matched group velocities. In this case, $|v_1|^2$ and $|v_2|^2$ propagate stably and hence a temporal optical Thirring soliton is realized. Panel (e) [(f)] is the result on the stability analysis of the temporal optical Thirring soliton, where E_1 (E_2) and $|\zeta_1|$ ($|\zeta_2|$) are energy and amplitude of the corresponding soliton component v_1 (v_2).

from (12) by taking $\zeta_0 = 1$, $\xi_0 = \eta_0 = \varphi_0 = 0$. To investigate the stability of the temporal Thirring soliton, perturbations are added to v_1 and v_2 so one has $v_1 = \text{sech}(\xi)(1 + \varepsilon\Psi_1)$ and $v_2 = \text{sech}(\xi)(1 + \varepsilon\Psi_2)$. Here ε is the amplitude of the perturbations and Ψ_1 and Ψ_2 are random variables uniformly distributed in the interval $[0, 1]$. Shown in Fig. 2(e) [Fig. 2(f)] is the energy $E_1 = \int |v_1|^2 d\xi$ ($E_2 = \int |v_2|^2 d\xi$) and the amplitude $|\zeta_1|$ ($|\zeta_2|$) of the soliton component v_1 (v_2) as functions of τ/τ_0 by taking $\varepsilon = 0.1$. We see that the energy (i.e., dashed red line) and the amplitude (i.e., solid blue line) of the soliton remain almost unchanged, which means that the optical Thirring soliton is stable during propagation.

Based on the system parameters given above, we can obtain the group velocities of the two polarization components of the probe pulse, which read

$$V_{g2} \approx V_{g1} \equiv V_g = 3.76 \times 10^{-4} c, \quad (13)$$

much smaller than the light speed c in vacuum, contributed by the EIT effect in the system. The input power density P for creating the temporal optical Thirring soliton predicted above can be estimated by using the Poynting's vector of the electromagnetic field [33]. The expression of the generation power of the soliton is given by $P = 2\varepsilon_0 c n_p S (\hbar/|\mathbf{p}_{14}|)^2 U_0^2$, where n_p is the refractive index and $S = \pi R^2$ is the cross-section area of the probe laser field. With the parameters used above, the input power of the temporal optical Thirring soliton reads

$$P \approx 9.24 \times 10^{-9} \text{ W}. \quad (14)$$

We see that, to generate the temporal optical Thirring soliton, a very low input light power is needed, which is due to the resonance character and the double EIT effect in the system, similarly to that found in Ref. [28].

IV. STERN-GERLACH DEFLECTION OF TEMPORAL OPTICAL THIRRING SOLITONS

We now turn to investigate the effect of the SG magnetic field, i.e., the external potential terms $\mathcal{M}_1 \xi v_1$ and $\mathcal{M}_1 \xi v_2$ play roles. In this case, with system parameters estimated above Eq. (10) reduces to

$$i \frac{\partial v_1}{\partial \tau} + \frac{1}{2} \frac{\partial^2 v_1}{\partial \xi^2} + |v_2|^2 v_1 + \mathcal{M}_1 \xi v_1 = 0, \quad (15a)$$

$$i \frac{\partial v_2}{\partial \tau} + \frac{1}{2} \frac{\partial^2 v_2}{\partial \xi^2} + |v_1|^2 v_2 + \mathcal{M}_2 \xi v_2 = 0. \quad (15b)$$

Due to the selected atomic energy levels mentioned above, we have $\mathcal{M}_1 = \mathcal{M}_2 = \mathcal{M}$. Introducing the transformation [36]

$$\tau' = \tau, \quad (16a)$$

$$\xi' = \xi - \frac{\mathcal{M}\tau^2}{2}, \quad (16b)$$

$$\phi_j(\tau', \xi') = v_j(\tau, \xi) e^{-i\mathcal{M}\tau(\xi - \mathcal{M}\tau^2/6)}, \quad (16c)$$

Eq. (15) is converted to the “free” temporal Thirring model,

$$i \frac{\partial \phi_1}{\partial \tau'} + \frac{1}{2} \frac{\partial^2 \phi_1}{\partial \xi'^2} + |\phi_2|^2 \phi_1 = 0, \quad (17a)$$

$$i \frac{\partial \phi_2}{\partial \tau'} + \frac{1}{2} \frac{\partial^2 \phi_2}{\partial \xi'^2} + |\phi_1|^2 \phi_2 = 0, \quad (17b)$$

which supports temporal optical Thirring solitons, as shown in Sec. III C. In particular, such solitons display trajectory deflection during propagation due to the presence of the SG gradient magnetic field.

Shown in Fig. 3 is the result of the numerical simulation for the propagation of a temporal optical Thirring soliton based on Eqs. (15) and (17), by taking the intensity $|\Omega_{p1}/U_0|^2$ (for σ^+ polarization component) and $|\Omega_{p2}/U_0|^2$ (for σ^- polarization component) as functions of x/R and z/L_{Diff} for different magnetic field gradient B . Shown in Fig. 3(a) [Fig. 3(b)] is the movement trajectory of the σ^+ polarization component $|\Omega_{p1}/U_0|^2$ (σ^- polarization component $|\Omega_{p2}/U_0|^2$) of the Thirring soliton for the SG magnetic field gradient $B = 32$ mG/mm (i.e., $\mathcal{M} = 0.01$) when it propagates to $z/L_{\text{Diff}} = 5, 10, 15, 20$, respectively. Figures 3(c) and 3(d) give a similar as that in Figs. 3(a) and 3(b) but for $B = 64$ mG/mm (i.e., $\mathcal{M} = 0.02$). We see that the Thirring soliton experiences a deflection under the action of the SG gradient magnetic field, and the deflection angle becomes larger when the magnetic field gradient B increases (or the value of \mathcal{M} is increased).

The analytical expression of the trajectory of the temporal optical Thirring soliton can be obtained by using the relations (7) and (16), which reads $(x, y, z) = (\frac{\mathcal{M}Rv_g^2}{2L_{\text{Diff}}^2}t^2, 0, V_g t)$. Thus the trajectory of the center position of the temporal optical Thirring soliton is given by

$$x = \frac{\mathcal{M}R}{2L_{\text{Diff}}^2} z^2, \quad (18)$$

which means that the soliton trajectory is a parabolic curve in the x - z plane. Shown in Fig. 4(a) is the deflection distance

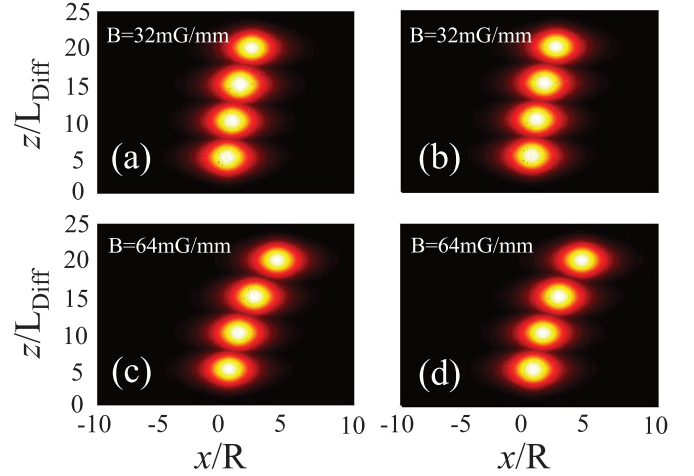


FIG. 3. Stern-Gerlach deflection of the temporal optical Thirring soliton by taking the intensity $|\Omega_{p1}/U_0|^2$ (for σ^+ polarization component) and $|\Omega_{p2}/U_0|^2$ (for σ^- polarization component) as functions of x/R and z/L_{Diff} for different magnetic field gradient B . Panel (a) [(b)] is the parabolic movement trajectory of the σ^+ polarization component $|\Omega_{p1}/U_0|^2$ (σ^- polarization component $|\Omega_{p2}/U_0|^2$) of the soliton for $B = 32$ mG/mm when it propagates to $z/L_{\text{Diff}} = 5, 10, 15, 20$, respectively. Panel (c) [(d)] is the same as panel (a) [(b)] but for $B = 64$ mG/mm. The trajectories of the center position of the optical Thirring soliton in all the four panels obey the parabolic formula $x/R = \mathcal{M}z^2/(2L_{\text{Diff}}^2)$.

x/R as a function of z/L_{Diff} for the magnetic field gradient $B = 32$ mG/mm (red dashed line) and $B = 64$ mG/mm (blue solid line), respectively. We see that the larger the magnetic field gradient B , the larger the deflection distance bending to the x direction.

It is easy to get the propagating velocity of the Thirring soliton

$$\mathbf{v} = \left(\frac{\mathcal{M}V_g^2 R}{L_{\text{Diff}}^2} t, 0, V_g \right). \quad (19)$$

Assume the soliton passes through the atomic medium with length L along the z direction. Thus the traveling time of the soliton in the z direction is $t = L/V_g$. Therefore, the velocity

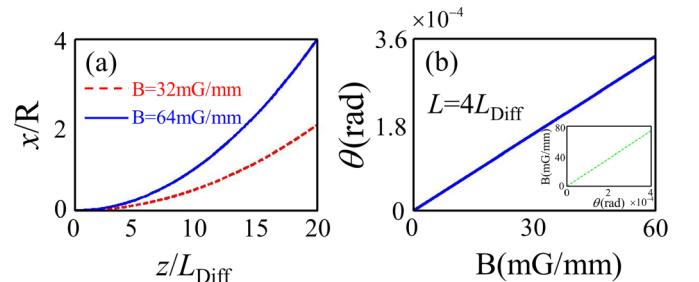


FIG. 4. Stern-Gerlach deflection distance and deflection angle θ of the temporal optical Thirring soliton. (a) Deflection distance x/R as a function of z/L_{Diff} for the magnetic field gradient $B = 32$ mG/mm (red dashed line) and $B = 64$ mG/mm (blue solid line), respectively. (b) Deflection angle θ as a function of the magnetic field gradient B when the soliton propagates to $z = 4L_{\text{Diff}} \approx 2.8$ cm. Inset: Magnetic field gradient B as a function of the deflection angle θ .

of the soliton at $z = L$ is given by $\mathbf{V} = (V_x, 0, V_g)$ with $V_x = \mathcal{M}R V_g L / L_{\text{Diff}}^2$. As a result, the soliton acquires the following deflection angle:

$$\theta = \frac{V_x}{V_g} = MR^2 \frac{L}{L_{\text{Diff}}} B, \quad (20)$$

when it propagates in the medium from $z = 0$ to $z = L$, where M has been defined in the Appendix A and its value has been given in Sec. III B.

Figure 4(b) shows the deflection angle of the Thirring soliton as a function of the SG gradient magnetic field B for propagation length $L = 4L_{\text{Diff}} \approx 2.8$ cm. We see that the larger magnetic field gradient B , the larger the deflection angle θ of the soliton. The deflection angle θ can reach to 10^{-4} radian when the magnetic field gradient $B = 32$ mG/mm ($B = 64$ mG/mm) for $L = 4L_{\text{Diff}}$, which is one order of magnitude larger than that of the dark-state polariton in a linear EIT system obtained in Ref. [37].

The SG effect of the temporal optical Thirring soliton demonstrated above may have many promising practical applications. One of them is the precision measurement of micro magnetic fields through the detection of the deflection angle of the soliton [see the inset of Fig. 4(b)]. In addition, based on the deflection one can design optical beam splitters and all-optical switching, etc. Since the system employed here can be actively manipulated through the selection of atomic levels and the adjustment of laser detunings, laser intensities, and other system parameters, such measurement can be made in a controllable way.

V. SUMMARY

In this work, we have proposed a physical scheme for the realization of an optical Thirring model and generation of the temporal optical Thirring solitons in a coherent tripod-type four-level atomic system. We have shown that under the

condition of the double EIT the optical Kerr nonlinearity of the system may be increased greatly and the CPM in the two polarization components of the probe laser pulse can be made to be much larger than the SPM, and thus the optical Thirring model can be obtained. Furthermore, we have shown that the system supports stable temporal optical Thirring solitons, which have ultralow generation power ($\sim 10^{-9}$ W) and ultraslow and well-matched propagation velocities ($\sim 10^{-4} c$). In particular, these temporal optical Thirring solitons may experience a Stern-Gerlach deflection and acquire a significant deflection angle when a gradient magnetic field is applied to the system. The theoretical method used in this work can be applied to investigate similar phenomena that may occur in other physical systems (e.g., laser-driven quantum wells). The results reported here are useful not only for extending the research realm of nonlinear magneto-optics but also for promising applications in the precision measurement of micromagnetic fields and for designing new optical devices useful in optical information processing and transmission.

ACKNOWLEDGMENTS

This work was supported by Natural Science Foundation of China under Grants No. 11704066, No. 11474099, and No. 61705034; the Science and Technology Project of Department of Education of Jiangxi Province under Grants No. GJJ160576 and No. GJJ160587; and the Natural Science Foundation of Jiangxi Province under Grant No. 20171BAB211007.

APPENDIX A: EQUATIONS OF MOTION FOR THE DENSITY-MATRIX ELEMENTS

The equation of motion for the density-matrix elements σ_{jl} reads [31]

$$i \frac{\partial}{\partial t} \sigma_{11} - i\Gamma_{14} \sigma_{44} + \Omega_{p1}^* \sigma_{41} - \Omega_{p1} \sigma_{41}^* = 0, \quad (\text{A1a})$$

$$i \frac{\partial}{\partial t} \sigma_{22} - i\Gamma_{24} \sigma_{44} + \Omega_{p2}^* \sigma_{42} - \Omega_{p2} \sigma_{42}^* = 0, \quad (\text{A1b})$$

$$i \frac{\partial}{\partial t} \sigma_{33} - i\Gamma_{34} \sigma_{44} + \Omega_c^* \sigma_{43} - \Omega_c \sigma_{43}^* = 0, \quad (\text{A1c})$$

$$i \left(\frac{\partial}{\partial t} + \Gamma_4 \right) \sigma_{44} + \Omega_{p1} \sigma_{41}^* + \Omega_{p2} \sigma_{42}^* + \Omega_c \sigma_{43}^* - \Omega_{p1}^* \sigma_{41} - \Omega_{p2}^* \sigma_{42} - \Omega_c^* \sigma_{43} = 0, \quad (\text{A1d})$$

$$\left(i \frac{\partial}{\partial t} + d_{21} \right) \sigma_{21} + \Omega_{p2}^* \sigma_{41} - \Omega_{p1} \sigma_{42}^* = 0, \quad (\text{A1e})$$

$$\left(i \frac{\partial}{\partial t} + d_{31} \right) \sigma_{31} + \Omega_c^* \sigma_{41} - \Omega_{p1} \sigma_{43}^* = 0, \quad (\text{A1f})$$

$$\left(i \frac{\partial}{\partial t} + d_{32} \right) \sigma_{32} + \Omega_c^* \sigma_{42} - \Omega_{p2} \sigma_{43}^* = 0, \quad (\text{A1g})$$

$$\left(i \frac{\partial}{\partial t} + d_{41} \right) \sigma_{41} + \Omega_{p1} (\sigma_{11} - \sigma_{44}) + \Omega_{p2} \sigma_{21} + \Omega_c \sigma_{31} = 0, \quad (\text{A1h})$$

$$\left(i\frac{\partial}{\partial t} + d_{42}\right)\sigma_{42} + \Omega_{p2}(\sigma_{22} - \sigma_{44}) + \Omega_{p1}\sigma_{21}^* + \Omega_c\sigma_{32} = 0, \quad (\text{A1i})$$

$$\left(i\frac{\partial}{\partial t} + d_{43}\right)\sigma_{43} + \Omega_c(\sigma_{33} - \sigma_{44}) + \Omega_{p1}\sigma_{31}^* + \Omega_{p2}\sigma_{32}^* = 0, \quad (\text{A1j})$$

where $d_{jl} = \Delta'_j - \Delta'_l + i\gamma_{jl}$ with $\Delta'_j = \Delta_j - \mu_{j1}Bx$, $\mu_{jl} = \mu_B(g_F^j m_F^j - g_F^l m_F^l)/\hbar$. Dephasing rates are defined as $\gamma_{jl} = (\Gamma_j + \Gamma_l)/2 + \gamma_{jl}^{\text{col}}$, with $\Gamma_j = \sum_{E_i < E_j} \Gamma_{ij}$ denoting spontaneous emission rate from the state $|j\rangle$ to all lower energy states $|i\rangle$ and γ_{jl}^{col} denoting the dephasing rate reflecting the loss of phase coherence between the states $|j\rangle$ and $|l\rangle$.

APPENDIX B: SOLUTIONS OF THE ASYMPTOTIC EXPANSION AT THE FIRST AND SECOND ORDERS

The first-order ($\alpha = 1$) solution of the asymptotic expansion is given by

$$\Omega_{pj}^{(1)} = F_j e^{i\theta_j}, \quad (\text{B1a})$$

$$\sigma_{3j}^{(1)} = -\frac{\Omega_c^* \sigma_{jj}^{(0)}}{D_j} F_j e^{i\theta_j}, \quad (\text{B1b})$$

$$\sigma_{4j}^{(1)} = \frac{(\omega + d_{3j}^{(0)})\sigma_{jj}^{(0)}}{D_j} F_j e^{i\theta_j}, \quad (\text{B1c})$$

with the envelopes F_j ($j = 1, 2$) depending on the slow variables x_1 , t_2 , and z_2 . Here $D_j = |\Omega_c|^2 - (\omega + d_{3j}^{(0)})(\omega + d_{4j}^{(0)})$ and $\theta_j = K_j(\omega)z_0 - \omega t_0$ [38], with

$$K_j(\omega) = \frac{\omega}{c} + \kappa_{j4} \frac{(\omega + d_{3j}^{(0)})\sigma_{jj}^{(0)}}{D_j} \quad (\text{B2})$$

the linear dispersion relations of the system, which have two branches with the imaginary of the both dispersion relations [i.e., $\text{Im}(K_j(\omega))$] displaying an EIT transparency window, a manifestation of the double EIT inherent in the tripod system. For more detail, see Ref. [30].

The second-order ($\alpha = 2$) solution reads

$$\sigma_{21}^{(2)} = \frac{\Omega_{p1}^{(1)}\sigma_{42}^{*(1)} - \Omega_{p2}^{*(1)}\sigma_{41}^{(1)}}{\omega + d_{21}^{(0)}}, \quad (\text{B3a})$$

$$\sigma_{43}^{(2)} = -\frac{\Omega_{p1}^{(1)}\sigma_{31}^{*(1)} + \Omega_{p2}^{(1)}\sigma_{32}^{*(1)}}{\omega + d_{43}^{(0)}}, \quad (\text{B3b})$$

with the other second-order density-matrix elements being zero.

Explicit expressions of the SPM and CPM coefficients W_{jl} appearing in Eq. (5) read

$$W_{11} = \kappa_{14} \frac{\Omega_c a_{431}^{*(2)}}{D_1}, \quad (\text{B4a})$$

$$W_{12} = \kappa_{14} \frac{[\omega + d_{31}^{(0)}]a_{21}^{(2)} + \Omega_c a_{432}^{*(2)}}{D_1}, \quad (\text{B4b})$$

$$W_{21} = \kappa_{24} \frac{[\omega + d_{32}^{(0)}]a_{21}^{*(2)} + \Omega_c a_{431}^{*(2)}}{D_2}, \quad (\text{B4c})$$

$$W_{22} = \kappa_{24} \frac{\Omega_c a_{432}^{*(2)}}{D_2}, \quad (\text{B4d})$$

with

$$a_{21}^{(2)} = \frac{1}{\omega + d_{21}^{(0)}} \left\{ \frac{[\omega + d_{32}^{*(0)}]\sigma_{22}^{(0)}}{D_2} - \frac{[\omega + d_{31}^{(0)}]\sigma_{11}^{(0)}}{D_1} \right\}, \quad (\text{B5a})$$

$$a_{431}^{(2)} = \frac{\Omega_c \sigma_{11}^{(0)}}{D_1 [\omega + d_{43}^{(0)}]}, \quad (\text{B5b})$$

$$a_{432}^{(2)} = \frac{\Omega_c \sigma_{22}^{(0)}}{D_2 [\omega + d_{43}^{(0)}]}. \quad (\text{B5c})$$

The coefficient M_j ($j = 1, 2$) contributed by the SG gradient magnetic field is given by

$$M_j = -\kappa_{j4} \frac{[\omega + d_{3j}^{(0)}]^2 \mu_{4j} + |\Omega_c|^2 \mu_{3j}}{2D_j^2}. \quad (\text{B6})$$

Due to the configuration symmetry of the tripod level structure, we have

$$M_2 \approx M_1 (\equiv M). \quad (\text{B7})$$

- [1] W. Thirring, A soluble relativistic field theory, *Ann. Phys.* **3**, 91 (1958).
 [2] H. B. Thacker, Exact integrability in quantum field theory and statistical systems, *Rev. Mod. Phys.* **53**, 253 (1981).
 [3] T. Bhattacharyya, Quantum integrability of bosonic massive Thirring model in continuum, *J. Math. Phys.* **46**, 012301 (2005).
 [4] K. Kravtsov, D. Rand, and P. R. Prucnal, Quantum theory of Thirring solitons, *Phys. Rev. A* **76**, 013812 (2007).

- [5] J. Yan and B.-L. Li, Functional integrals and convergence of partition function in Sine-Gordon-Thirring model, *Lett. Math. Phys.* **104**, 233 (2014).
 [6] N. Joshi and D. E. Pelinovsky, Integrable semi-discretization of the massive Thirring system in laboratory coordinates, *J. Phys. A: Math. Theor.* **52**, 03LT01 (2019).
 [7] L. V. Belvedere and E. C. Marino, Superconducting Thirring model, *Phys. Rev. D* **37**, 2354 (1988).

- [8] L. V. Belvedere, Mass versus superconducting-gap generation: The operator formulation for $N = 2$, *Phys. Rev. D* **41**, 2622 (1990).
- [9] L. V. Belvedere and E. C. Marino, Exact solution of the O(2) symmetric Thirring model with dynamical generation of a superconducting gap, *J. Phys. A: Math. Gen.* **23**, 205 (1990).
- [10] I. F. Herbut, V. Juricic, and B. Roy, Theory of interacting electrons on the honeycomb lattice, *Phys. Rev. B* **79**, 085116 (2009).
- [11] W. Armour, S. Hands, and C. Strouthos, Monte Carlo simulation of the semimetal-insulator phase transition in monolayer graphene, *Phys. Rev. B* **81**, 125105 (2010).
- [12] L. Janssen and H. Gies, Critical behavior of the (2+1)-dimensional Thirring model, *Phys. Rev. D* **86**, 105007 (2012).
- [13] B. H. Wellegehausen, D. Schmidt, and A. Wipf, Critical flavor number of the Thirring model in three dimensions, *Phys. Rev. D* **96**, 094504 (2017).
- [14] G. Lenz, P. Meystre, and E. M. Wright, Nonlinear Atom Optics, *Phys. Rev. Lett.* **71**, 3271 (1993).
- [15] G. Lenz, P. Meystre, and E. M. Wright, Nonlinear atom optics: General formalism and atomic solitons, *Phys. Rev. A* **50**, 1681 (1994).
- [16] O. Zobay, S. Pötting, P. Meystre, and E. M. Wright, Creation of gap solitons in Bose-Einstein condensates, *Phys. Rev. A* **59**, 643 (1999).
- [17] O. Cohen, T. Carmon, M. Segev, and S. Odoulov, Holographic solitons, *Opt. Lett.* **27**, 2031 (2002).
- [18] O. Cohen, M. M. Murnane, and H. C. Kapteyn, Cross-phase-modulation nonlinearities and holographic solitons in periodically poled photovoltaic photorefractives, *Opt. Lett.* **31**, 954 (2006).
- [19] S. Trillo, Resonance Thirring solitons in type II second-harmonic generation, *Opt. Lett.* **21**, 1732 (1996).
- [20] H. He and P. D. Drummond, Ideal Soliton Environment Using Parametric Band Gaps, *Phys. Rev. Lett.* **78**, 4311 (1997).
- [21] H. He and P. D. Drummond, Theory of multidimensional parametric band-gap solitons, *Phys. Rev. E* **58**, 5025 (1998).
- [22] Z. Toroker and M. Horowitz, Study of quasi-elastic Bragg soliton collisions in uniform fiber Bragg gratings by using the solution of the massive Thirring model, *J. Opt. Soc. Am. B* **27**, 1195 (2010).
- [23] Q. Zhou, Q. Zhu, Y. Liu, H. Yu, P. Yao, and A. Biswas, Thirring optical solitons in birefringent fibers with spatio-temporal dispersion and Kerr law nonlinearity, *Laser Phys.* **25**, 015402 (2015).
- [24] Q. Zhou, Y. Zhong, M. Mirzazadeh, A. H. Bhrawy, E. Zerrad, and A. Biswas, Thirring combo-solitons with cubic nonlinearity and spatio-temporal dispersion, *Waves Ran. Comp. Med.* **26**, 204 (2016).
- [25] S. T. R. Rizvi, S. Salim, K. Ali, and M. Younis, New Thirring optical solitons with vector-coupled Schrödinger equations in birefringent fibers, *Waves Ran. Comp. Med.* **27**, 359 (2017).
- [26] I. Friedler, G. Kurizki, O. Cohen, and M. Segev, Spatial Thirring-type solitons via electromagnetically induced transparency, *Opt. Lett.* **30**, 3374 (2005).
- [27] S. Jana and S. Konar, A new family of Thirring type optical spatial solitons via electromagnetically induced transparency, *Phys. Lett. A* **362**, 435 (2007).
- [28] H. Li and K. Zhang, Spatial soliton pairs of the vectorial Thirring model realized in a coherent atomic system via electromagnetically induced transparency, *Phys. Rev. A* **95**, 013829 (2017).
- [29] Y. Qi, Y. Niu, F. Zhou, H. Sun, and S. Gong, Thirring-type spatial optical solitons in asymmetric quantum wells, *J. Phys. B: At. Mol. Opt. Phys.* **51**, 025504 (2018).
- [30] Y. Chen, Z. Chen, and G. Huang, Storage and retrieval of vector optical solitons via double electromagnetically induced transparency, *Phys. Rev. A* **91**, 023820 (2015).
- [31] R. W. Boyd, *Nonlinear Optics*, 3rd ed. (Academic, San Diego, CA, 2008).
- [32] D. A. Steck, Rubidium 87 D Line Data, <http://steck.us/alkalidata/>.
- [33] G. Huang, L. Deng, and M. G. Payne, Dynamics of ultraslow optical solitons in a cold three-state atomic system, *Phys. Rev. E* **72**, 016617 (2005).
- [34] Y. Guo, L. Zhou, L. Kuang, and C. P. Sun, Magneto-optical Stern-Gerlach effect in an atomic ensemble, *Phys. Rev. A* **78**, 013833 (2008).
- [35] J. Liu, C. Hang, and G. Huang, Weak-light vector rogue waves, breathers, and their Stern-Gerlach deflection via electromagnetically induced transparency, *Opt. Express* **25**, 23408 (2017).
- [36] Z. Chen and G. Huang, Trapping of weak signal pulses by soliton and trajectory control in a coherent atomic gas, *Phys. Rev. A* **89**, 033817 (2014).
- [37] L. Karpa and M. Weitz, A Stern-Gerlach experiment for slow light, *Nat. Phys.* **2**, 332 (2006).
- [38] The frequency of the probe field is $\omega_p + \omega$, and the wave number of the j th polarization component is $k_p + K_{pj}(\omega)$. Thus $\omega = 0$ corresponds to the center frequency of the probe field.